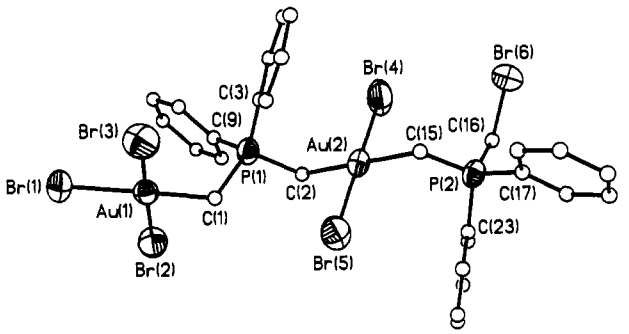

Figure 2. Drawing of the structure of **5**. Thermal ellipsoids have been drawn at the 50% probability level. Carbon atoms are of arbitrary radii for clarity. The solvent molecule is not shown.

176.0 (2)-179 (1)°. Nothing unusual is observed in the geometries of the ylide ligands. The gold-halogen bond lengths, particularly those of complex **5**, are of interest.

With regard to the gold-halogen bond lengths, we have recently described two conformers of the trans/trans complex **3**, one that crystallized[3b] in the space group $C2/c$ with an interstitial molecule of $CDCl_3$ and one that crystallized[7] in $P2_1/c$ with no solvent molecule. In the $C2/c$ structure, two bromine atoms are tilted toward a semibridging position and the measured Au-Br bonds are 2.411 (3) and 2.440 (3) Å. However, in the $P2_1/c$ structure, a trigonal-bipyramidal distortion of the geometry of Au atoms is observed in which the Au-Br bond lengths are significantly longer, 2.535 (4) and 2.576 (4) Å. The latter distortion was attributed[7] to the intramolecular interaction of the two Au^{III} atoms, which were separated by a 3.069 (2) Å distance.

The comparative study of the $C2/c$ and $P2_1/c$ structures of **3** raised the question of choosing a standard Au^{III}-Br bond length against which the *trans*-Br-Au-Br units can be compared. We believe that the bond lengths measured around Au(2) of structure **5** can be accepted as standard for a *trans*-$Au^{III}Br_2$ bond. This gold atom has a coordination identical with that of the gold atoms of **3**, two trans ylides and two trans bromides, while its geometry is not disturbed by any other interactions. The Au(2)-Br bonds measured in **5**, 2.406 (6) and 2.420 (5) Å, are in good agreement with the bond lengths of the $C2/c$ structure of **3**, confirming our previous assumption that the latter bonds lengths are not affected by intramolecular Br···Br interactions.

The Au(1)-Br(1) bond of **5**, trans to the ylide ligand and cis to the other bromides, is very long, 2.479 (6) Å, reflecting the trans influence of the $-CH_2-$ group. The cis/cis isomer[4] of **3** also has long Au-Br bonds, 2.497 (4) and 2.487 (5) Å, as does as the cis side of the cis/trans complex[3c] $[Au(CH_2)_2PPh_2]_2(CH_2CF_3)Br_3$, 2.470 (3) and 2.476 (4) Å. Also, the Au-Cl bond lengths of **4** are in good agreement with the bond lengths measured in the structure of the cis/trans isomer[3b] of **2**. The cis side of the latter structure has Au-Cl bonds of 2.338 (9) and 2.360 (7) Å. The 2.357 (5) Å Au(1)-Cl(2) bond of **4** falls in this range, while the trans side of *cis/trans*-**2** has Au-Cl bonds of 2.295 (9) and 2.272 (9) Å, similar to the ones measured in the *trans*-$AuCl_2$ units of **4**.

We have mentioned (vide supra) that the reactions[3c] of ICl and Br_2 with the Au^{III} A-frame complexes $(\mu\text{-}CH_2)[Au(CH_2)_2PPh_2]_2X_2$ cleave the Au-(μ-CH_2) bonds, not the Au-CH_2(ylide) bonds, with formation of dihalomethanes. This preferential reactivity has been used[11] to synthesize mixed-ligand complexes such as *trans/trans*-$[Au(CH_2)_2PPh_2]_2(CN)_2X_2$ (X = Cl, Br) obtained from the reaction of $(\mu\text{-}CH_2)[Au(CH_2)_2PPH_2]_2(CN)_2$ with ICl and Br_2, respectively.

Acknowledgment. We acknowledge with thanks the financial support for this work from the National Science Foundation (Grant CHE8708625) and the Robert A. Welch Foundation.

Supplementary Material Available: Tables SI-SIX, listing crystallographic data, bond lengths, bond angles, anisotropic thermal parameters, and hydrogen positional parameters for **4** and **5** (11 pages); Tables SX and SXI, listing observed and calculated structure factors for **4** and **5** (59 pages). Ordering information is given on any current masthead page.

Contribution from the Groupe de Spectroscopie des Complexes Polymétalliques et de Métalloprotéines and Groupe Structure, Service de Physique, Département de Recherche Fondamentale (DRF) du Centre d'Etudes Nucléaires de Grenoble (CENG), 85X, Grenoble 38041, France, and Université Joseph Fourier, Grenoble, France

Influence of a Phase Transition in the Solid State on the Structure of a Synthetic Iron-Sulfur Cubane

P. Excoffon,*[,†,‡] J. Laugier,[§] and B. Lamotte*[,‡]

Received July 23, 1990

The tetranuclear iron-sulfur cubane compound $[Bu_4N]_2[Fe_4S_4(SC_6H_5)_4]$, which is a good model for the active sites of ferredoxins, presents a phase transition at 243 K between two solid phases called phase I and phase II. The crystallographic structure of phase II having been previously described, we report here, in order to compare them, the structure of phase I at 233 K. Its space group is orthorhombic $P2na$, with a = 11.888 (5) Å, b = 23.21 (1) Å, c = 22.22 (1) Å, $\alpha = \beta = \gamma = 90°$. The structure has been refined for 5866 reflections, 3697 of which were greater than $2\sigma(I)$. The final values are R = 0.044, R_w = 0.057. The phase transition has been studied and is found to be of the first order. It presents a small hysteresis, and its total entropy gain is ΔS = 7.5 J K^{-1} mol^{-1}. In the two phases and principally in phase I the cubane core is distorted from T_d symmetry, the distortion not being describable as a D_{2d} compression. The phase transition does not appear to be driven by the geometry changes appearing at the cubane core level. Rather, the origin of this phase transition must be due to an increase of disorder at the butyl ends of the counterions and to simultaneous changes of the orientations of the benzenethiolate ligands. Thus, we view the changes of geometry and symmetry appearing at the level of the cubane core as essentially shaped by its immediate environment, within the limits of plasticity that this structure admits.

I. Introduction

Iron-sulfur cubanes are interesting clusters since they constitute the active site of numerous metalloproteins involved in electron-transfer biological processes.[1-3] In order to understand their properties, Holm and co-workers[4] have created and studied ex-

† Universite Joseph Fourier.
‡ Groupe de Spectroscopie des Complexes Polymétalliques et de Métalloprotéines.
§ Groupe Structure.

(1) Lovenberg, W., Ed. *Iron Sulfur Proteins* Academic Press: New York, 1977.
(2) Spiro, T. G., Ed. *Iron Sulfur Proteins* John Wiley and Sons, Inc.: New York, 1982.
(3) *Iron Sulfur Protein Research*; Matsubara, Hiroshi, Katsube, Yukiteru, Wada, Keishiro, Eds.; Japan Scientific Societies Press: Tokyo, 1987.

0020-1669/91/1330-3075$02.50/0

Table I. Comparison of Crystal Data for Phases I and II of Bis(tetra-*n*-butyl ammonium)tetrakis[(benzenethiolato)-(μ_3-sulfido)iron]: $[Bu_4N]_2[Fe_4S_4(SPh)_4]$

	phase I	phase II
temp, K	233K	291K
mol wt	1273.2	
a, Å	11.888 (5)	11.984 (9)
b, Å	23.21 (1)	23.524 (4)
c, Å	23.22 (1)	23.686 (3)
α, deg	90	
β, deg	90	91.78 (3)
γ, deg	90	
V, Å^3	6406.9	6674.1
space group	*P2na*	$P2_1/n$

tensively their synthetic analogues ligated by different thiolate groups. The properties of these compounds have been discussed in relation to their geometries determined by X-ray crystallography. In this article, we take the opportunity of the previous observation of a phase transition in a compound of this family[5] to compare the geometry of the cubane core in the two phases and to discuss the origin of the phase transition.

A previous EPR study[5] of paramagnetic states induced by gamma irradiation in single crystals of the $[Bu_4N]_2[Fe_4S_4(S\text{-}Ph)_4]$ compound has shown that this crystal undergoes a structural transition at 243 K between a low-temperature phase called here phase I and a high-temperature phase called here phase II. The structure of phase II has been previously determined at room temperature, and is described in ref 5. It is monoclinic and corresponds to the $P2_1/n$ space group. On the other hand, until now, the structure of phase I was unknown. Its description and comparison with the structure of phase II is the subject of the present article.

We have found it interesting to attempt such a study and such a comparison for two reasons:

(i) Comparisons of the geometry of the Fe_4S_4 cores have already been made for the same anion in the two different redox state $[Fe_4S_4]^{2+}$ and $[Fe_4S_4]^{+}$.[4c-e] Moreover, other comparisons of this geometry have been made for cores in the same redox state but with different ligands and (or) counterions.[4b-h,6-12] We have thought, owing to the opportunity offered by this phase transition, that it would be interesting to compare cores that exist in two different crystallographic structures for the same compound the same $[Fe_4S_4]^{2+}$ redox state.

(ii) On this occasion, a new and interesting question arises that we will answer here: Is the change of geometry of the cubane core driving the phase transition or not?

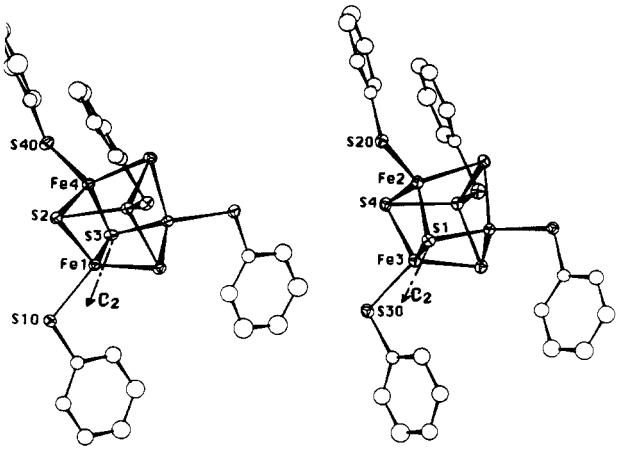

ANION 1 ANION 2

Figure 1. Structure of the two cores with their ligands in phase I at 233 K. Anion 1 corresponds to the Wyckoff 2*a* position and anion 2 to the Wyckoff 2*b* position.

II. Study of the Structure of Phase I

(a) X-ray Data Collection and Reduction. We have obtained small crystals of $[Bu_4N]_2[Fe_4S_4(SPh)_4]$ from J. Gloux, who has prepared this compound by the usual procedure.[13]

Well-formed black crystals of about 0.2 × 0.25 × 0.2 mm were selected and sealed under argon in quartz capillaries. They were tested at room temperature by using Laue diffraction and precession techniques. Intensity data were obtained on a Nonius-CAD4 four-circle diffractometer with a graphite-crystal monochromator (Mo Kα; λ = 0.71069 Å).

The crystal temperature was controlled by a nitrogen gas jet between 173 and 295 K with a precision better than 1 K. In order to avoid the mosaic effect that occurs close to the phase transition temperature, the sample was slowly cooled (0.1 K/mn) and kept for $^1/_2$ h at a fixed temperature before collecting data. We have thus tested the reversibility of the measurements in phase I. It was not possible to do the same in phase II because the crystal was broken by mosaic effects upon warming through the transition.

A total of 5866 reflections was collected at 233 K. The raw data were reduced to net intensities. Standard deviations were calculated on the basis of counting statistics. Lorentz-polarization corrections were applied, and equivalent reflections were averaged. The atom scattering factors were taken from ref 14. In view of the small μ values, no absorption correction was applied. Finally, 3697 independent structure factors with $F > 2\sigma(F)$ were selected.

(b) Structure Determination. Crystallographic parameters and selection rule considerations indicate two possible space groups for phase I: *P2na* and *Pmna*.

The structure of phase I was solved with the help of the previously solved phase II structure.[5] It was supposed that the phase transition does not change considerably the crystallographic arrangement, since the cell parameters are not greatly modified (Table I). In order to determine first the heavy-atom positions, we have considered the Fe and S atomic positions of the cubane Fe_4S_4 in phase II, and searched for an appropriate translation *T* in relation to the new symmetry. We have found

$$T = (-0.18, -0.25, -0.25)$$

P2na with *Z* = 4 is the only space group that satisfies the structure of the cubane, the crystallographic symmetries, and the compound density measured in phase II. In this group, the gravity centers of the Fe_4S_4 cubanes must reside at the special Wyckoff positions 2*a* and 2*b* on the C_2 axis:[14]

$$2a: \ (x, 0, 0); \ (\tfrac{1}{2} + x, 0, \tfrac{1}{2})$$

$$2b: \ (x, \tfrac{1}{2}, 0); \ (\tfrac{1}{2} + x, \tfrac{1}{2}, \tfrac{1}{2})$$

The asymmetric part of the structure was solved with two independent half-anions. The structure was refined by the least-squares method

(4) (a) Herskovitz, T.; Averill, B. A.; Holm, R. H.; Ibers, J. A.; Philipps, W. D.; Weiher, J. F. *Proc. Natl. Acad. Sci. U.S.A.* **1972**, *69*, 2437–2441. (b) Averill, B. A.; Herskovitz, T.; Holm, R. H.; Ibers, J. A. *J. Am. Chem. Soc.* **1973**, *95*, 3523–3534. (c) Que, L.; Bobrik, M. A.; Ibers, J. A.; Holm, R. H. *Ibid.* **1974**, *96*, 4168–4178. (d) Frankel, R. B.; Averill, B. A.; Holm, R. H. *J. Phys., Colloq.* **1974**, *C6*, 107–112. (e) Laskowski, E. J.; Frankel, R. B.; Gillum, W. O.; Papaefthymiou, G. C.; Renaud, J.; Ibers, J. A.; Holm, R. H. *J. Am. Chem. Soc.* **1978**, *100*, 5322–5337. (f) Laskowski, E. J.; Reynolds, J. G.; Frankel, R. B.; Foner, S.; Papaefthymiou, G. C.; Holm, R. H. *Ibid.* **1979**, *101*, 6562–6570. (g) Berg, J. M.; Hodgson, K. O.; Holm, R. H. *Ibid.* **1979**, *101*, 4586–4591. (h) Mascharak, P. K.; Hagen, K. S.; Spence, J. T.; Holm, R. H. *Inorg. Chim. Acta* **1983**, *80*, 157–170. (i) Johnson, R. E.; Papaefthymiou, G. C.; Frankel, R. B.; Holm, R. H. *J. Am. Chem. Soc.* **1983**, *105*, 7220–7287.
(5) Gloux, J.; Gloux, P.; Hendriks, H.; Rius, G. *J. Am. Chem. Soc.* **1987**, *109*, 3220–3224.
(6) Ollerenshaw, T. J.; Garner, C. D.; Odell, B.; Clegg, W. *J. Chem. Soc., Dalton Trans.* **1985**, 2161–2165.
(7) O'Sullivan, T.; Millar, M. M. *J. Am. Soc.* **1985**, *107*, 4096–4097.
(8) Carrel, H. L.; Glusker, J. P.; Job, R.; Bruice, T. C. *J. Am. Chem. Soc.* **1977**, *99*, 3683.
(9) Christou, G.; Garner, C. D.; Drew, M. G. B.; Cammak, R. *J. Chem. Soc., Dalton Trans.* **1981**, 1550–1555.
(10) Ueyama, N.; Sugawara, T.; Fuji, M.; Nakamura, A.; Yasuoka, N. *Chem. Lett.* **1985**, 175–178.
(11) Coucouvanis, D.; Kanatzidis, M.; Simhon, E.; Baenziger, N. C. *J. Am. Chem. Soc.* **1982**, *104*, 1874–1882.
(12) Kanatzidis, M. G.; Coucouvanis, D.; Simopoulos, A.; Kostikas, A.; Papaefthymiou, G. C. *J. Am. Chem. Soc.* **1985**, *107*, 4925–4930.
(13) Christou, G.; Garner, C. D. *J. Chem. Soc., Dalton Trans.* **1979**, 1093.
(14) *International Tables for X-ray Crystallography*; Kynoch Press: Birmingham, England, 1974; Vol. IV.

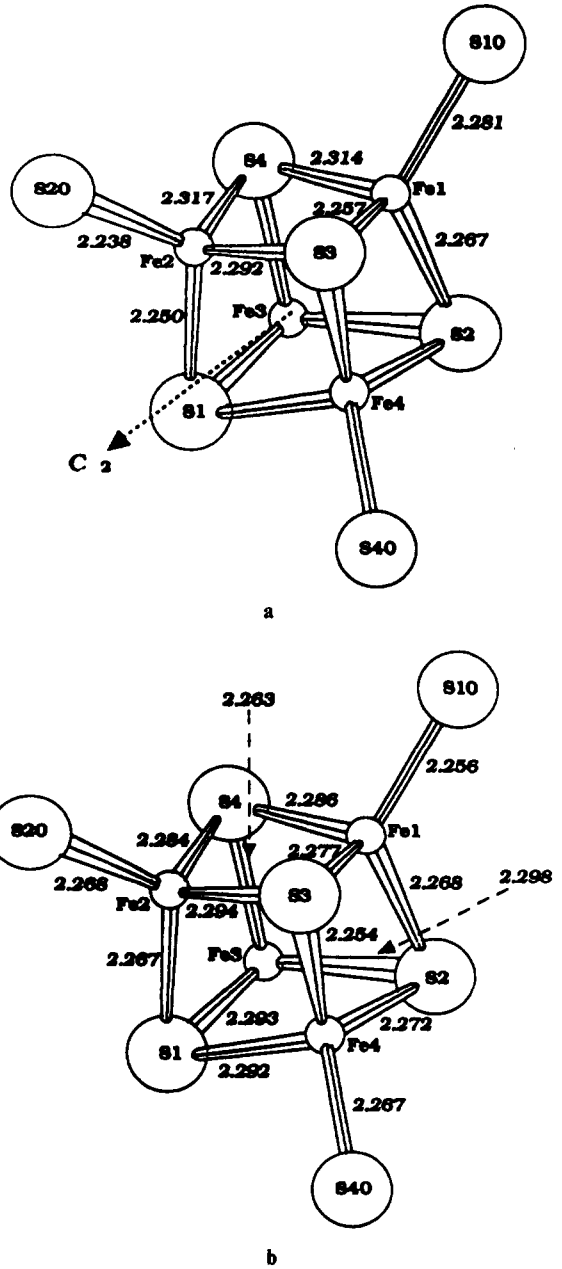

Figure 2. Comparison of the core geometries of $[Fe_4S_4]S_4^*$ in the two phases: (a) in phase I at 233 K (for core at the 2*a* position); (b) in phase II at 295 K.

(Shelx 76).[15] The first atomic coordinates of the heavy atoms (four irons, 8 sulfurs) were taken from the phase II structure[5] with the translation defined above. With only the heavy atoms included, R was equal to 0.25. Other non-hydrogen atoms were located from subsequent Fourier electron density difference maps. Four $[Bu_4N]^+$ cations in the unit cell have thus been located on the crystallographically imposed 2-fold axis, while the other four cations were located in general positions.

The limited data set (3697 for 638 parameters) required that the phenyl rings be constrained to a D_{6h} symmetry with the C–C distances equal to 1.392 Å. They were allowed to have individual, variable isotropic thermal parameters. Anisotropic temperature factors were assigned for all other non-hydrogen atoms.

At this point of the refinement we obtained $R = 0.062$ and the difference Fourier map clearly showed two quasi-equal maxima densities indicating disorder of the terminal carbon atom of a butyl chain with an occupation probability of 0.5 for each position. In this case, the R factor dropped to 0.058.

A final refinement included calculated hydrogen atoms (except for terminal methyl hydrogens) and gave $R = 0.044$ ($R_w = 0.057$) (Tables I–III and supplementary material).

Another refinement with a data set of 3307 reflections at 170 K gave $R = 0.045$ and $R_w = 0.048$.

(15) Sheldrick, G. Shelx 76 System of Computing Programs. University of Cambridge, England, 1976.

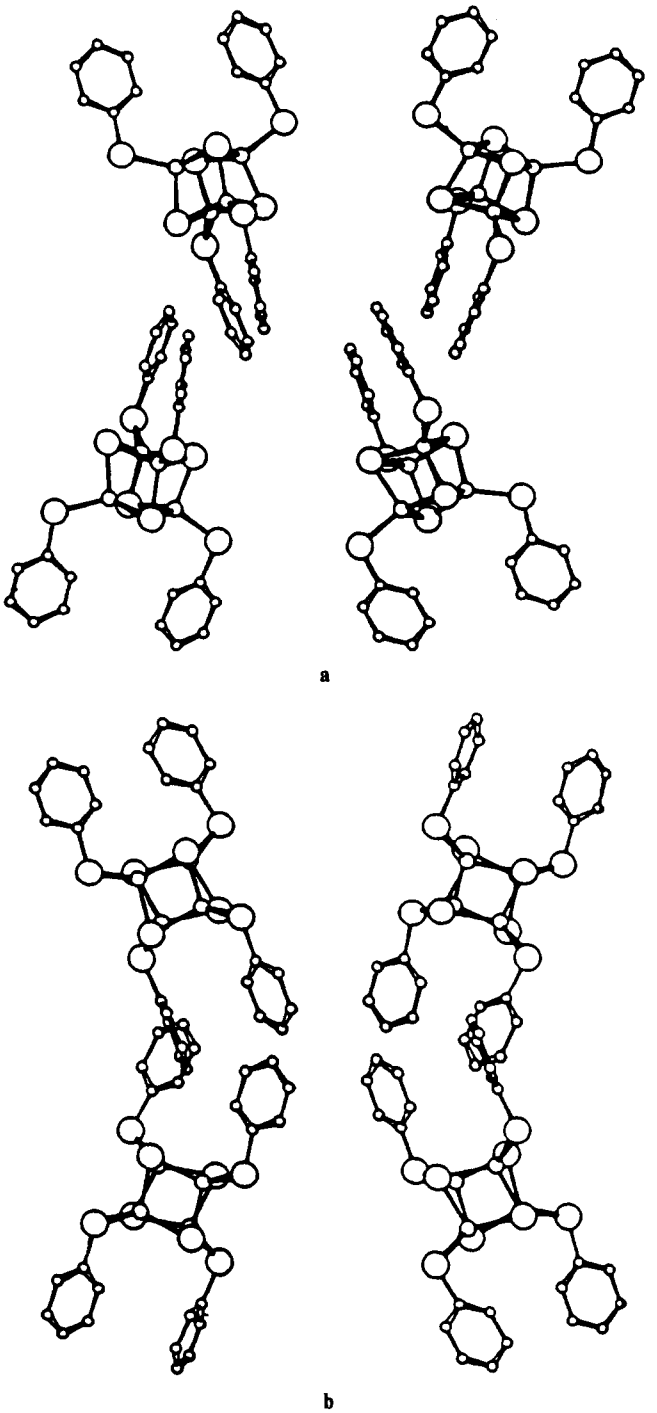

Figure 3. Comparison of the relative orientations of the phenyl planes of the thiolate ligands in the two phases: (a) in phase I at 233 K; (b) in phase II at 295 K.

III. Comparisons of the Structure of the Two Phases

The result obtained is that phase I is orthorhombic with the space group *P2na*, while phase II has previously been found to be monoclinic with the space group $P2_1/n$.[5] Thus, at first glance, the crystal symmetry is lower in the high-temperature phase than in the low-temperature phase, in opposition to what is generally found in structural phase transitions. Figure 1 shows the structure of the two cores with their ligands in phase I.

Table I presents the comparison of the crystallographic data relative to the unit cell for phases I and II, while Table II gives the atomic positions in phase I and Table III gives the elements of comparison for the cubane core in both phases. Figures 2–4

Table II. Atomic Positions, Thermal Parameters, and Standard Deviations (in Parentheses) for the Atoms of $[Bu_4N]_2[Fe_4S_4(SPh)_4]$ in Phase I (Except Hydrogens) at 233 K[a]

	x	y	z	B_{EQ}, Å^2		x	y	z	B_{EQ}, Å^2
				Half-Anion 1					
Fe1	7421 (0)	5230 (1)	543 (1)	3.16	C14	7641 (6)	4671 (3)	2492 (3)	7.56
Fe4	5810 (2)	4458 (1)	223 (1)	3.20	C15	7654 (6)	4963 (3)	1966 (3)	5.98
S2	7722 (3)	4292 (1)	318 (1)	3.45	C16	8552 (6)	5325 (3)	1830 (3)	4.14
S3	5557 (3)	5280 (1)	720 (1)	3.53	C21	14313 (6)	11135 (3)	3366 (3)	5.11
S10	8621 (3)	5681 (1)	1163 (1)	4.20	C22	14354 (6)	11261 (3)	2779 (3)	7.01
S40	4644 (3)	3711 (1)	345 (1)	4.47	C23	15251 (6)	11577 (3)	2555 (3)	7.85
C11	9437 (6)	5395 (3)	2218 (3)	5.38	C24	16107 (6)	11768 (3)	2919 (3)	7.36
C12	9423 (6)	5104 (3)	2743 (3)	6.05	C25	16066 (6)	11642 (3)	3506 (3)	5.59
C13	8525 (6)	4742 (3)	2880 (3)	7.65	C26	15169 (6)	11325 (3)	3730 (3)	3.93
				Half-Anion 2					
Fe2	13873 (2)	9505 (1)	5310 (1)	3.33	C44	5600 (7)	3465 (4)	2009 (4)	9.77
Fe3	12254 (1)	9692 (1)	4499 (1)	3.53	C45	5592 (7)	3666 (4)	1443 (4)	7.19
S1	14144 (3)	9597 (1)	4327 (1)	3.67	C46	4734 (7)	3499 (4)	1068 (4)	4.54
S4	12041 (3)	9342 (1)	5415 (1)	3.88	C31	12144 (6)	10215 (3)	6965 (3)	6.51
S20	15165 (3)	11184 (1)	4470 (1)	3.93	C32	12180 (6)	9977 (3)	7516 (3)	6.34
S30	11048 (3)	10794 (1)	6063 (1)	4.46	C33	11227 (6)	9991 (3)	7866 (3)	6.10
C41	3885 (7)	3131 (4)	1260 (4)	7.52	C34	10237 (6)	10243 (3)	7664 (3)	8.27
C42	3893 (7)	2931 (4)	1826 (4)	9.22	C35	10201 (6)	10481 (3)	7113 (3)	6.85
C43	4751 (7)	3097 (4)	2201 (4)	9.02	C36	11154 (6)	10467 (3)	6763 (3)	4.03
				Half-Cation 1 with N at x, 0.5, 0					
N1	1638 (13)	5000 (0)	0 (0)	4.08	C121	905 (12)	4606 (5)	325 (5)	4.02
C111	2456 (13)	5325 (5)	411 (5)	4.68	C122	1476 (13)	4166 (6)	715 (6)	5.73
C112	1843 (12)	5622 (5)	914 (5)	4.86	C123	580 (15)	3835 (7)	1095 (8)	8.46
C113	2665 (13)	6029 (5)	1205 (5)	5.67	C124	979 (28)	3386 (12)	1436 (11)	7.14
C114	2186 (13)	6315 (5)	1752 (5)	6.23	C125	28 (29)	4078 (15)	1468 (11)	8.74
				Half-Cation 2 with N at x, 0, 0.5					
N2	8060 (14)	0 (0)	5000 (0)	4.92	C221	7304 (12)	9618 (5)	4632 (5)	4.36
C211	8903 (14)	9627 (6)	5378 (5)	5.31	C222	7831 (14)	9234 (7)	4238 (6)	6.76
C212	8245 (14)	9254 (7)	5812 (6)	6.92	C223	7002 (13)	8846 (6)	3929 (6)	6.19
C213	9141 (14)	8792 (8)	6030 (7)	9.75	C224	7544 (19)	8426 (8)	3508 (7)	10.10
C214	9521 (17)	8337 (8)	5603 (10)	10.80					
				Cation 3 in General Position					
N3	2976 (8)	2506 (3)	5558 (4)	4.84	C331	2049 (10)	2906 (4)	5765 (5)	4.75
C311	2618 (11)	2212 (5)	4983 (5)	5.21	C332	969 (12)	2603 (5)	5956 (6)	6.10
C312	2207 (22)	2590 (6)	4520 (6)	9.17	C333	190 (12)	3062 (5)	6226 (6)	6.61
C313	2287 (23)	2308 (6)	3953 (7)	9.75	C334	611 (15)	3370 (6)	6768 (6)	7.57
C314	3045 (24)	2518 (8)	3583 (11)	13.89	C341	3254 (13)	2028 (5)	5998 (6)	5.96
C321	4005 (11)	2883 (5)	5442 (6)	6.01	C342	3685 (15)	2252 (7)	6586 (7)	8.43
C322	5040 (12)	2562 (6)	5253 (8)	8.05	C343	4068 (17)	1781 (7)	6979 (7)	8.95
C323	6069 (15)	2874 (7)	5313 (8)	9.20	C344	4646 (21)	2002 (9)	7509 (9)	12.22
C324	7153 (14)	2611 (7)	5107 (8)	8.39					

[a] Further details are given in the supplementary material.

illustrate the comparison for, respectively, the cubane core geometry, the relative disposition of the phenyl groups of the thiolate ligands in the crystal, and the geometry of the tetrabutylammonium ions.

Let us now discuss the main facts emerging from this comparison of the two phases.

(a) The structure of the cubane core is of higher symmetry in phase I than in phase II since in the first case the different atoms are related by a C_2 axis while no symmetry element is present for the cubane in phase II, as can be seen in Figure 2a,b. However, the cubane dimensions are rather similar; the small changes in distances which appear will be discussed in more detail in section V.

(b) The orientations of the phenyl rings in the benzenethiolate ligands change between the two phases: in phase I, they are packed nearly parallel two by two on opposite sides of a $Fe_4S_4(SPh_4)$ group and they pile up and interpenetrate each other between neighbors like a "key and lock system"[16] (see Figure 3a). In constrast, the projection shown in Figure 3b illustrates that this relatively tight disposition is lost in phase II since some planes of the phenyl groups are tilted with respect to the others.

(c) The most apparent differences between the two phases concern the tetrabutylammonium cations. Their comparison is shown in Figure 4. In phase I, the cations are present in three different types of sites in the unit cell: cation 1 with N at (x = 0.1638, y = 0.5, z = 0), cation 2 with N at x = 0.8060, y = 0, z = 0.5), and cation 3 in a general position (see Table II and Figure 4a). In this phase, the positions of all of the carbon atoms of the butyl groups are well-defined, except for the cation with its nitrogen centered on (x = 0.1638, y = 0.5, z = 0), which exhibits disorder for two terminal carbons related by the C_2 symmetry centered on the nitrogen atom.

In contrast, in Phase II, the disorder of these terminal carbons of tetrabutylammonium cations is greatly increased, as can be seen in Figure 4b. One cation has one terminal methyl group disordered between two positions. For the other cations, one butyl group has the same disorder as the previous one, while the opposite butyl group has its third and fourth carbon disordered.

These results indicate that the factor apparently driving the phase transitions must be related to the increase of disorder due to thermal motion of the butyl chain groups and especially of their extremities, which have inherently large degrees of freedom and are only constrained by crystal packing forces. This can be seen in more detail by looking at the isotropic thermal temperature factors of the carbon atoms of the butyl groups in the two phases (Table I). These temperature factors increase generally from the first carbon bound to nitrogen to the terminal one in each of the methyl groups. Moreover, these temperature factors are generally greater in phase II than in phase I. This fact is naturally in good

(16) Guthrie, G. B.; McCullough, J. P. *J. Phys. Chem. Solids* **1961**, 18.

Table III. Comparison of Selected Distances (Å) and Angles (deg) of the $(Fe_4S_4)^{2+}$ Core in the Two Phases[a] (Phase II at $T = 295$ K and Phase I (for the Core at the 2*a* Position) at 233 K)

	phase I	phase II
	(a) Distances	
Fe1–Fe2	2.712 (3)	2.746 (4)
Fe3–Fe4	2.712 (3)	2.726 (4)
Fe1–Fe3	2.738 (6)	2.740 (4)
Fe2–Fe4	2.721 (6)	2.714 (4)
Fe1–Fe4	2.726 (3)	2.728 (4)
Fe2–Fe3	2.726 (3)	2.749 (4)
S1–S2	3.663 (5)	3.630 (6)
S3–S4	3.663 (5)	3.609 (6)
S1–S3	3.587 (7)	3.606 (6)
S2–S4	3.603 (7)	3.594 (6)
S1–S4	3.571 (5)	3.573 (6)
S2–S3	3.571 (5)	3.562 (6)
Fe1–S2	2.267 (5)	2.268 (5)
Fe1–S3	2.257 (3)	2.277 (5)
Fe1–S4	2.314 (5)	2.286 (5)
Fe3–S4	2.267 (5)	2.263 (5)
Fe3–S1	2.257 (3)	2.293 (5)
Fe3–S2	2.314 (5)	2.298 (5)
Fe2–S3	2.292 (5)	2.294 (5)
Fe2–S4	2.316 (4)	2.284 (5)
Fe2–S1	2.250 (4)	2.267 (5)
Fe4–S1	2.292 (5)	2.292 (5)
Fe4–S2	2.316 (4)	2.272 (5)
Fe4–S3	2.250 (4)	2.254 (5)
	(b) Angles	
Fe1–Fe2/Fe1–Fe3	60.0 (1)	60.13 (9)
Fe1–Fe2/Fe1–Fe4	60.0 (1)	59.44 (9)
Fe1–Fe2/Fe2–Fe3	60.5 (1)	59.83 (9)
Fe1–Fe2/Fe2–Fe4	60.2 (1)	59.94 (9)
Fe1–Fe2/Fe3–Fe4	90.1 (1)	89.53 (9)
Fe1–Fe3/Fe1–Fe4	59.5 (1)	59.81 (9)
Fe1–Fe3/Fe2–Fe3	59.5 (1)	60.04 (9)
Fe1–Fe3/Fe2–Fe4	89.6 (2)	89.94 (9)
Fe1–Fe3/Fe3–Fe4	60.0 (1)	59.87 (9)
Fe1–Fe4/Fe2–Fe3	90.7 (1)	89.59 (9)
Fe1–Fe4/Fe2–Fe4	59.7 (1)	60.62 (9)
Fe1–Fe4/Fe3–Fe4	60.5 (1)	60.33 (9)
Fe2–Fe3/Fe2–Fe4	59.7 (1)	59.87 (9)
Fe2–Fe3/Fe3–Fe4	60.0 (1)	59.43 (9)
Fe2–Fe4/Fe3–Fe4	60.2 (1)	60.70 (9)
S1–S2/S1–S3	59.7 (1)	59.0 (2)
S1–S2/S1–S4	59.7 (1)	59.9 (2)
S1–S2/S2–S3	59.4 (1)	60.2 (2)
S1–S2/S2–S4	58.9 (1)	59.3 (2)
S1–S2/S3–S4	90.7 (1)	88.9 (2)
S1–S3/S1–S4	61.6 (1)	60.4 (2)
S1–S3/S2–S3	61.6 (1)	60.8 (2)
S1–S3/S2–S4	87.0 (1)	88.3 (2)
S1–S3/S3–S4	59.0 (1)	59.4 (2)
S1–S4/S2–S3	87.8 (1)	89.3 (2)
S1–S4/S2–S4	61.4 (1)	60.9 (2)
S1–S4/S3–S4	59.4 (1)	60.3 (2)
S2–S3/S2–S4	61.4 (1)	60.6 (2)
S2–S3/S3–S4	59.8 (1)	60.2 (2)
S2–S4/S3–S4	58.9 (1)	59.3 (2)

agreement with the appearance of higher degree of disorder at the chain ends in phase II.

The same kind of observations on temperature factors can also be made concerning the atoms of the benzenethiolate ligands. They also present a general increase of these temperature factors between the sulfur bound to the iron and the carbons at the other end of the phenyl groups, and their values are generally higher in phase II than in phase I.

Moreover, the anisotropic thermal parameters determined for the $(Fe_4S_4(SPh)_4)^{2-}$ anion in phase II[5] show that the phenyl planes exhibit a marked tendency to rotate along an axis joining the terminal para ring carbon and the carbon bound to the thiolate sulfur, as indicated by the largest temperature factors in the ellipsoids corresponding to carbons in ortho and meta positions in these phenyl rings. This fact is certainly related to the less compact arrangement of the phenyl rings in phase II than in phase I, which has been put into evidence above.

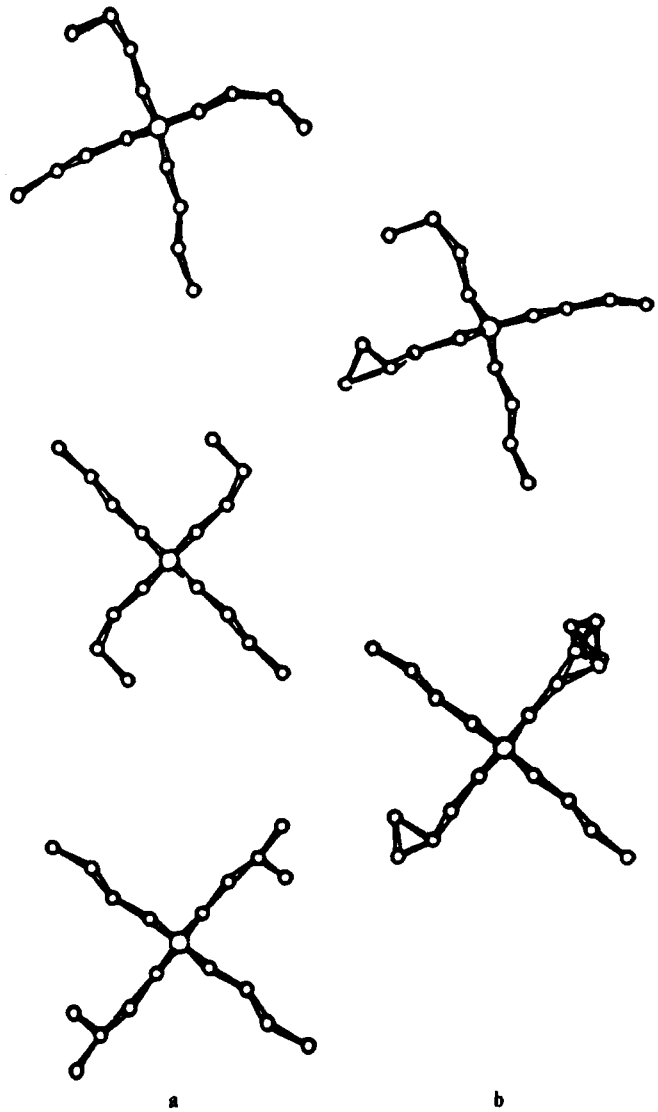

Figure 4. Comparison of the geometries of the $(Bu_4N)^+$ cations and of the disorder of their butyl chains in the two phases: (a) in phase I at 233 K; (b) in phase II at 295 K.

Thus, it appears that the cause of the phase transition is primarily related to the increase of disorder appearing at the level of the terminal carbons of certain butyl chains of the cations. But the methylene and methyl groups of these chains are in contact with the phenyl rings of the thiolate ligands and in fact these two kinds of chemical groups certainly interact strongly, these movements gaining in freedom and amplitude when going from phase I to phase II.

Finally, we find that a higher symmetry of the low-temperature phase with respect to the high-temperature phase is not abnormal here, since we are dealing with a first-order transition that is not a Landau transition. In a Landau transition, the high-temperature phase includes all the symmetry elements of the low-temperature phase and possesses in addition a supplementary symmetry element. Then the high-temperature phase is unavoidably of higher symmetry. However, this obligation disappears in the case of a first-order transition between two phases that correspond to two rather different organizations of the molecular and ionic structures, each one having symmetry elements different from the other.

IV. Analysis of the Phase Transition

The temperature variations of the *a*, *b*, and *c* parameters of the unit cell have been determined along both sides of the phase

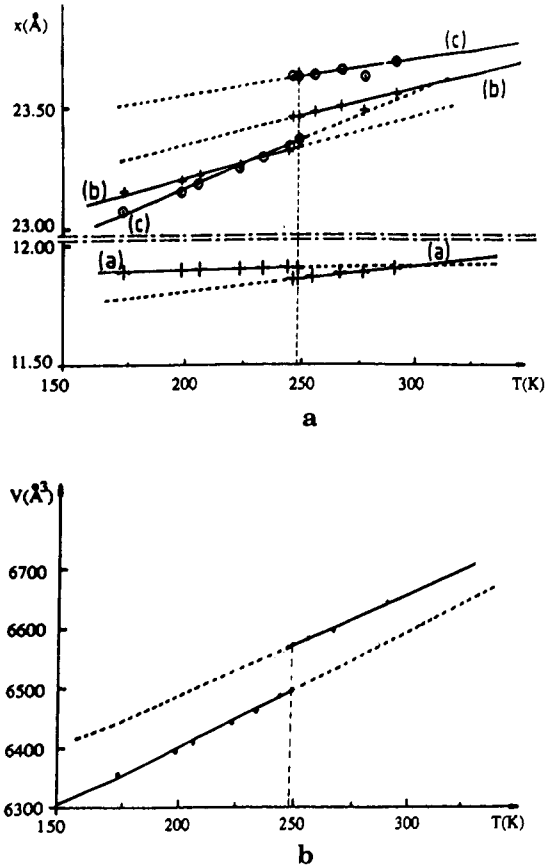

Figure 5. Temperature dependence of crystallographic parameters between $T = 150$ K and $T = 300$ K (through the phase transition): (a) temperature variation of the unit cell parameters a, b, and c; (b) temperature variation of the unit cell volume V. The expansion thermal coefficients $\chi_i(X) = (1/X)(\Delta X/T)$ (in 10^{-4} K^{-1}) of phase I have been calculated from these results: $\chi_I(a) = 0$, $\chi_{II}(a) = 1$, $\chi_I(b) = 1.1$, $\chi_{II}(b) = 1.24$, $\chi_I(c) = 1.9$, $\chi_{II}(c) = 0.84$. At the phase transition, the relative discontinuity is −0.45% for the a parameter, 0.5% for the b parameter, and 1% for the c parameter. Consequently, including the discontinuity of the β angle, the relative discontinuity on the unit cell volume is 1.1%.

transition. They are reported in Figure 5, which also shows the volume variation occurring at the phase transition. The discontinuity of these parameters show that this transition is first order. The variations of the parameters are certainly mainly related to the increased disorder and correlated wagging of the butyl groups and also to the geometric reorganization of the phenyl groups occurring at the phase transition when going from phase I to phase II. We observed that the crystal was generally broken upon warming up through the phase transition. We also observed an hysteresis-like behavior in the measurements around the transition temperature. But this phenomenom may be due to a nucleation effect related to the fact that it is possible, by rapid freezing at 77 K, to keep the phase II monoclinic structure at this temperature.

Moreover, thermodynamic measurements have been made at the phase transition by differential scanning calorimetry, which give a value for the total entropy gain, ΔS, of 7.5 J K^{-1} mol^{-1} [17] confirming thus that it is a first-order transition.

One can try to relate this experimental value to the increase of disorder found above for the carbon atoms of the butyl groups by calculating $\Delta S = -R \log (N_1/N_2)$ where R is the ideal gas constant (8.32 J K^{-1} mol^{-1}) and N_1 and N_2 are the numbers of independent configurations found respectively in phases I and II. In this calculation, we have to take into account the fact that the probability occupancies for some of the disordered carbon positions are different from 0.5 and may range from 0.3 to 0.7. We find that such a calculation gives a value larger than the experimental one. In our opinion, this discrepancy indicates that the position of the disordered carbons at the butyl ends (in phase II) are somehow correlated. These correlations would be mediated by chemical groups in contact with the butyl end groups within the crystal, i.e. especially the phenyl groups.

Finally, we have verified that the Mössbauer spectra of the cubanes between the two phases do not change appreciably (for phase II, the Mössbauer spectrum has been taken at low temperature after a rapid freeze of the sample; under these experimental conditions, the monoclinic phase is frozen out and kept, even at very low temperature). Thus, at the limit of resolution of these spectra, the isomeric shifts and quadrupolar couplings are the same in the two phases, and we have found that their temperature dependences are also the same. This indicates that the changes in the geometry of the cubane and of its immediate surroundings are unsufficient to give rise to any significant changes at the level of the iron atoms detectable by Mössbauer spectroscopy.

V. Discussion of the Fe_4S_4 Core Geometry in the Two Phases

It has already been noted[5] that, in phase II, the geometry of the cubane (and especially its Fe–S* distances) does not follow the model of a compressed $[Fe_4S_4]^{2+}$ core of apparent D_{2d} symmetry, as Holm and al. previously reported for similar cubanes in the same redox state.[4] Our results on phase I—illustrated in Figure 2a—confirm this fact and even increase this discrepancy. Indeed, we find that the average Fe–S* distances are almost the same in both phases (2.283 Å in phase I and 2.279 Å in phase II). However, the structure is more distorted in phase I since the mean deviation of Fe–S* distances is 0.025 Å compared with 0.012 Å in phase II. In fact, the distorted cubane of phase I presents approximately the same differences between Fe–S* bond distances as those found for other cubanes reported in ref 4. However, it cannot, in any sense, be described as a compressed core along a (even approximative) D_{2d} axis. It also cannot be compressed along the C_2 symmetry axis that it possesses in this phase.

Let us first examine more closely the cubane structure in phase I. In this phase, the crystallographic structure imposes a C_2 symmetry axis onto the Fe_4S_4 cores. Within a precision on distances of better than 1%, the iron tetrahedra agree with the T_d symmetry group. But this is not the case for the sulfur tetrahedra, which, hence, are less symmetric. We find however (see Table IIIa,b) that these sulfur tetrahedra agree with D_{2d} symmetry (within a precision on S–S distances of better than 1% and a precision on angles better than 0.7%). But we must point out that if the iron and sulfur tetrahedra agree respectively with T_d symmetry and D_{2d} symmetry, they do not have a common $\bar{4}$ axis, even if a $\bar{4}$ axis of the iron tetrahedra is very close to the $\bar{4}$ axis of the sulfur tetrahedra. This is why iron–sulfur distances differ between them and why we must discard the global D_{2d} symmetry for the cubane. We find that these (just defined above) $\bar{4}$ axes are orthogonal to the C_2 crystallographic axis. They are also perpendicular to the Fe1–Fe2, Fe3–Fe4, S1–S2, and S3–S4 directions. We must note that the considerations developed above hold as well for the core located at the 2a Wyckoff position, as well as for the one located at the 2b position.

In spite of the small values of the numbers involved, the distortion apparent at the level of the Fe–S* distances may possibly be rationalized in the following way: in the same cubane, it is possible to pass from the $\bar{4}$ axis of the sulfur tetrahedron to the $\bar{4}$ axis of the iron tetrahedron (the closest to the previous one) by a combination of two geometrical transformations. The first one would be a translation along the C_2 axis of 0.03 Å (for the cores at the 2a and 2b Wyckoff positions) and the second one a rotation around the same C_2 axis of 0.4° for the core at the 2a position and of 0.2° for the core at the 2b position.

Coming now to the examination of the cubane structure in phase II, we find that no constraint is imposed by crystalline symmetry on the Fe_4S_4 core in this case. However, relying on the same precision on angles and distances as above, we find that the iron and sulfur tetrahedra agree independently with the D_{2d} symmetry in this phase. However, their $\bar{4}$ axes corresponding to each iron and sulfur tetrahedron in each cubane are not superimposed. In

(17) This measurement was obtained by J. Gloux (private communication).

this phase, they cross at their common center of gravity, but differ by a 0.5° rotation. They are nearly perpendicular, respectively, to the $\bar{4}$ and C_2 axes considered in phase I. Finally, we must note that, at a lower precision (1.3% on distances and 2% on angles), the iron and the sulfur tetrahedra both agree with the T_d symmetry in phase II. Within the same precision, only the iron tetrahedra agree with this T_d symmetry in phase I.

Thus, it seems that overall, as the temperature is decreased through the phase transition, the structure behaves as if the iron tetrahedra were trying to approach T_d symmetry, at the expense of the organization of the "softer" sulfur atoms. Apparently, the supplementary distortion of the Fe_4S_4 core introduced by this temperature change must be a consequence of the strains due to the reorganization of the phenyls of the thiolate ligands and of the chain ends of the tetrabutylammonium ions, which drive the phase transition. However, these geometrical changes at the level of cubane cores are of small amplitude and they have no apparent influence on the electronic structure of the cubane, which, as seen by Mössbauer spectroscopy, remains the same in the two phases.

VI. Conclusion

The origin of the phase transition appears to be due to an increase of the dynamic disorder at the level of the terminal carbon atoms of the tetrabutylammonium counterions. These motional changes possibly drive, via intermolecular interactions, the observed partial reorganization of the relative orientations of the phenyl planes of the thiolate groups.

Concerning the structure of the cubane itself, we think that it is its immediate environment that imposes its low symmetry and modulates its geometry. Finally, we think that the geometry modification between the two phases must result from the interplay of the external influences exercised by the vicinal ligands and counterions and of its rather rigid internal structure, which presents however some plasticity. The geometric changes observed at the level of the cubane cores have no apparent influence on the electronic state of the system.

Acknowledgment. We thank all persons of the DRF who helped us with technical facilities and stimulating discussions. We want to thank especially P. Auric, who performed Mössbauer experiments, and B. Castaing for useful discussions on thermodynamic theory.

Registry No. $[Bu_4N]_2[Fe_4S_4(SC_6H_5)_4]$, 52586-83-1.

Supplementary Material Available: Tables of crystallographic data, positional and thermal parameters for all atoms, and angles and distances for bonds between them (32 pages); a listing of observed and calculated structure factors (18 pages). Ordering information is given on any current masthead page.

Contribution from the Istituto di Teoria e Struttura Elettronica dei Composti di Coordinazione del CNR, Area della Ricerca di Roma, P.O. Box 10, 00016 Monterotondo Stazione, Roma, Italy

Metal Complexes of the New Ligand 1,2,6,7-Tetracyano-3,5-diimino-3,5-dihydropyrrolizinide, $M^{II}(C_{11}N_7H_2)_2$, as Basic Units for Molecular Materials. Electrochemical and Metal–Phthalocyanine-Like Electronic Properties of the Nickel(II) Complex and X-ray Crystal Structures of Its Adducts with Dioxane and Tetrathiafulvalene

Mario Bonamico, Vincenzo Fares,* Alberto Flamini,* and Nicola Poli

Received October 17, 1990

The synthesis, characterization, and electrochemical behavior of the bis(1,2,6,7-tetracyano-3,5-diimino-3,5-dihydropyrrolizinido)nickel(II) complex, Ni(β-dtpy)$_2$, have been investigated. In solution it is square planar and shows a metal–phthalocyanine-like electronic structure. In the solid state it incorporates oxygenated solvent of crystallization and the nickel is hexacoordinated, as from the results of the reported X-ray crystal structure of $Ni(C_{11}N_7H_2)_2 \cdot 2H_2O \cdot 3diox$ (**3**) (diox = 1,4-dioxane). The crystal structure of the TTF and THF adduct, $Ni(C_{11}N_7H_2)_2 \cdot TTF \cdot 2THF$ (**4**), is also reported: it is a charge-transfer complex, consisting of infinite stacks of alternate donor and acceptor molecules. Both complexes crystallize in the monoclinic system. Crystal data are as follows: for **3**, $C_{34}H_{32}N_{14}NiO_8$, space group $P2_1/n$, a = 11.184 (3) Å, b = 15.682 (4) Å, c = 11.720 (4) Å, β = 110.77 (2)°, Z = 2; for **4**, $C_{36}H_{24}N_{14}NiO_2S_4$, space group $P2_1/c$, a = 11.920 (3) Å, b = 21.612 (8) Å, c = 7.979 (2) Å, β = 109.68 (2)°, Z = 2. The cyclic voltammetry of Ni(β-dtpy)$_2$ shows multistep, overlapping reduction waves from 0 to −1.5 V vs SCE. A very small concentration of the radical monoanion $Ni(\beta\text{-dtpy})_2^{\bullet-}$ can be generated in solution, as detected by EPR spectroscopy during in situ electrolysis in DMF with $LiClO_4$ as supporting electrolyte (unresolved structure signal, g = 2.0057). Nevertheless the radical monoanion can be quantitatively isolated in the solid state as $Ni(\beta\text{-dtpy})_2^{\bullet-}Et_4N^+ \cdot 3CH_3OH$ (**6**) when the electrolysis of Ni(β-dtpy)$_2$ is carried out in methanol with TEAP as supporting electrolyte. **6** is a semiconductor ($\sigma = 1.062 \times 10^{-4}$ S cm^{-1}; E_a = 0.024 eV) with the unpaired electrons partially antiferromagnetically coupled at room temperature (μ_{eff} = 1.36 μ_B). As far as the delocalization of the odd electron in $Ni(\beta\text{-dtpy})_2^{\bullet-}$ anion is concerned, both the ESR and ESCA data of **6** show that it is confined mainly to the ligand system.

1. Introduction

After our discovery[1] that the polycyanopyrrolenine anion (**1**), resulting from a reductive autocondensation of tetracyanoethylene[2] (TCNE), reacts with divalent metal ions yielding bis(β-diiminotetracyanopyrrolizinido)metal(II) complexes M(β-dtpy)$_2$ (**2**)[3] (Scheme I), we began to study complexes **2** with the aim of evaluating them as basic units for producing molecular materials such as one-dimensional conducting charge-transfer compounds, on the analogy of tetracyanoquinodimethane (TCNQ), for the

(1) Bonamico, M.; Fares, V.; Flamini, A.; Poli, N. *Angew. Chem., Int. Ed. Engl.* **1989**, *28*, 1049.
(2) Dessy, G.; Fares, V.; Flamini, A.; Giuliani, A. M. *Angew. Chem., Int. Ed. Engl.* **1985**, *24*, 426.
(3) Numbering of the compounds throughout this paper is as follows: $C_{11}N_7H_2^-$ (**1**); $M(C_{11}N_7H_2)_2 \equiv M(\beta\text{-dtpy})_2$ (**2**); $Ni(\beta\text{-dtpy})_2 \cdot 2H_2O \cdot 3diox$ (**3**); $Ni(\beta\text{-dtpy})_2 \cdot TTF \cdot 2THF$ (**4**); $Ni(\beta\text{-dtpy})_2 \cdot 2C_3H_6O$ (**5**); $Ni(\beta\text{-dtpy})_2^{\bullet-}NEt_4^+ \cdot 3CH_3OH$ (**6**); $Ni(\beta\text{-dtpy})_2 \cdot 2THF \cdot 2THF$ (**7**); $Cu(\beta\text{-dtpy})_2 \cdot 2THF$ (**8**); $Et_3NH^+TCNQ^{\bullet-}$ (**9**).

0020-1669/91/1330-3081$02.50/0